ROYAL SOCIETY OF CHEMISTRY

EDGE ARTICLE

Check for updates

All publication charges for this article have been paid for by the Royal Society of Chemistry

Methyl scanning approach for enhancing the biological activity of the linear peptidic natural product, efrapeptin C†

Yuanqi Lin,[a] Hiroaki Itoh, [ID] [a] Shingo Dan [ID] [b] and Masayuki Inoue [ID] *[a]

Efrapeptin C (**1a**) is a large peptidic natural product comprising a 15-mer linear sequence and exerts potent anticancer activity by inhibiting mitochondrial F_oF_1-ATP synthase. Residues 1–6 and 9–15 of **1a** fold into two 3_{10}-helical domains and interact with ATP synthase, while the central β-Ala-7–Gly-8 region functions as a flexible linker of the two domains. To enhance the function of **1a** by minimally modifying its structure, we envisioned attaching one small methyl group to the β-Ala-7–Gly-8 and designed six methylated analogues **1b–1g**, differing only in the position and configuration of the methyl group. We enabled the first solid-phase total synthesis of **1a** and unified syntheses of **1b–1g**. The growth inhibitory activities of **1a–1g** against MCF-7 cells varied significantly: **1f** with (*S*)-β[3]-hAla-7 and its epimer **1g** with (*R*)-β[3]-hAla-7 were 4-fold more and 5-fold less potent, respectively, than **1a**. Remarkably, the most potent **1f** had the most stabilized 3_{10}-helical conformation and the highest hydrophobicity, which likely contributed to its effective transfer to the target protein within mitochondria. Moreover, **1f** exhibited higher proteolytic stability than **1a**. Therefore, the present methyl scanning approach provides a new strategy for changing the original properties of linear peptidic natural products to develop new pharmaceuticals.

Introduction

Numerous peptidic natural products have been characterized from bacteria, fungi, plants, and animals. These peptides have been evolutionarily optimized for a certain function and many of them display significant biological activities. Accordingly, these compounds often serve as drugs or as lead structures for the discovery of new pharmaceuticals.[1–3] Potent and selective bioactivities originate from large linear or cyclic architectures comprising various unusual monomers, including non-proteinogenic amino acids. Among peptidic natural products, cyclic peptides are intensively investigated by medicinal chemists because the macrocycle generally preorganizes the peptide conformation and functional group orientations for target-binding interactions.[4–8] Linear peptides, on the other hand, have been considered less suitable for drug development due to their higher conformational freedom than cyclic peptides and lability toward proteolytic enzymes.

Efrapeptin C (**1a**, Fig. 1) is a linear peptidic natural product with a molecular weight of 1607.[9,10] Compound **1a** was isolated from cultures of an ascomycete fungus, *Tolypocladium inflatum*,

and structurally determined to possess an N-terminal acetyl group (Ac-cap), 15 hydrophobic amino acid residues, and a C-terminal cationic heterocycle (C-cap) with the 1,5-diazabicyclo[4.3.0]non-5-ene (DBN) structure. The sequence comprises seven α-aminoisobutyric acids (Aib-2, -4, -5, -9, -10, -12, and -15), three L-pipecolic acids (L-Pip-1, -3, and -11), two L-leucines (L-Leu-6 and -14), two glycines (Gly-8 and -13), and one β-alanine (β-Ala-7). Thus, 11 of the 15 amino acids are non-proteinogenic residues.

Although **1a** is toxic to various species, such as bacteria, fungi, and insects,[11] potent anticancer activity is its most pharmacologically valuable feature. For example, a mixture of **1a** and its natural congeners displays strong growth inhibitory activity against human breast cancer MCF-7 cells [50% inhibitory concentration (GI_{50}) = 27 nM], and shows 60% growth inhibition at a dose of 0.15 mg kg^{-1} in mice xenografted with MCF-7 cells.[12]

Compound **1a** exerts its activity by binding to F_oF_1-ATP synthase in mitochondria and inhibiting ATP synthesis in oxidative phosphorylation (OXPHOS).[13–16] An X-ray analysis reported by Walker (Fig. 2a)[17] demonstrated that **1a** interacts with the F_1 subunit of F_oF_1-ATP synthase and decreases nucleotide binding affinity for ATP synthesis. Upon binding, the Aib-rich residues 1–6 and 9–15 of **1a** adopt 3_{10}-helical conformations by forming hydrogen bonding networks between the carbonyl oxygen of residue-(*i*) and the NH group of residue-(*i* + 3). In this bound form, the central β-Ala-7–Gly-8 with no branched alkyl group serves as a flexible linker and organizes the two helical

[a]*Graduate School of Pharmaceutical Sciences, The University of Tokyo, 7-3-1 Hongo, Bunkyo-ku, Tokyo 113-0033, Japan. E-mail: inoue@mol.f.u-tokyo.ac.jp*

[b]*Division of Molecular Pharmacology, Cancer Chemotherapy Center, Japanese Foundation for Cancer Research, 3-8-31 Ariake, Koto-ku, Tokyo 135-8550, Japan*

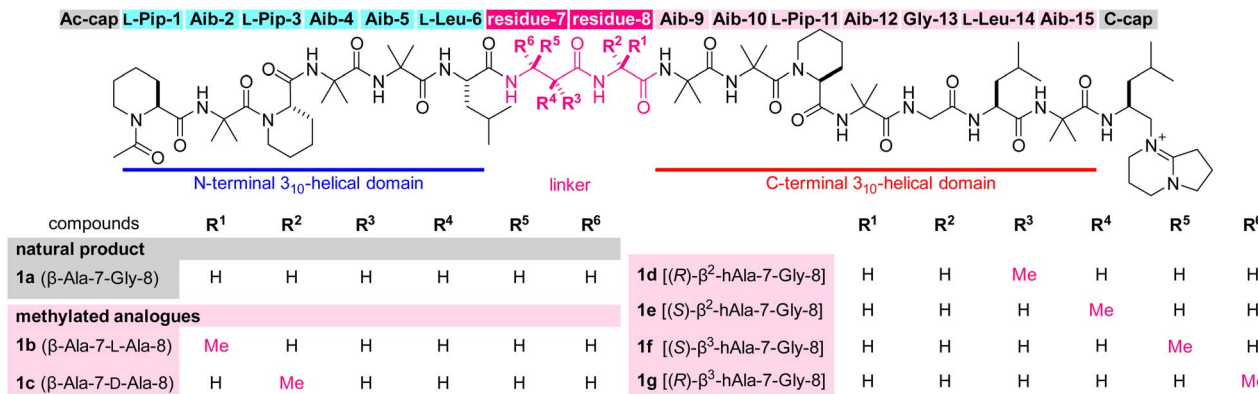† Electronic supplementary information (ESI) available. See DOI: https://doi.org/10.1039/d4sc04384g

| | Ac-cap | L-Pip-1 | Aib-2 | L-Pip-3 | Aib-4 | Aib-5 | L-Leu-6 | residue-7 | residue-8 | Aib-9 | Aib-10 | L-Pip-11 | Aib-12 | Gly-13 | L-Leu-14 | Aib-15 | C-cap |

N-terminal 3_{10}-helical domain — linker — C-terminal 3_{10}-helical domain

compounds	R^1	R^2	R^3	R^4	R^5	R^6			R^1	R^2	R^3	R^4	R^5	R^6
natural product														
1a (β-Ala-7-Gly-8)	H	H	H	H	H	H	1d	[(R)-β²-hAla-7-Gly-8]	H	H	Me	H	H	H
methylated analogues							1e	[(S)-β²-hAla-7-Gly-8]	H	H	H	Me	H	H
1b (β-Ala-7-L-Ala-8)	Me	H	H	H	H	H	1f	[(S)-β³-hAla-7-Gly-8]	H	H	H	H	Me	H
1c (β-Ala-7-D-Ala-8)	H	Me	H	H	H	H	1g	[(R)-β³-hAla-7-Gly-8]	H	H	H	H	H	Me

Fig. 1 Structures of efrapeptin C (**1a**) and its mono-methylated analogues **1b–1g**. The abbreviations for amino acids of residues 7–8 are also displayed with the compound numbers. Aib = 2-aminoisobutyric acid, hAla = homoalanine, Pip = pipecolic acid.
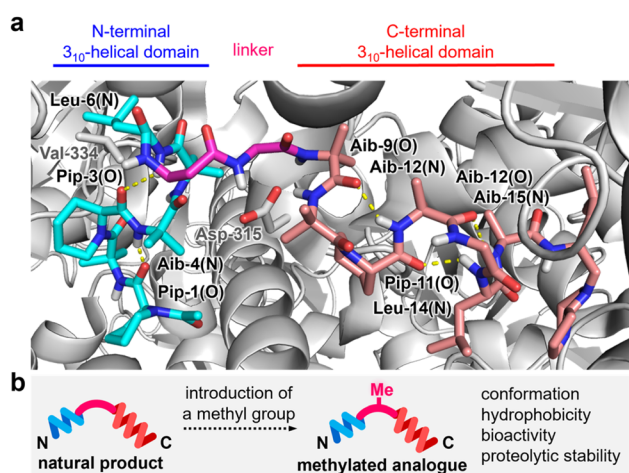

Fig. 2 (a) Intramolecular hydrogen bonds (yellow dotted lines) of **1a** in complex with the F_1 domain of bovine F_oF_1-ATP synthase (PDB ID: 1EFR). N-terminal and C-terminal 3_{10}-helical domains are highlighted in cyan and pink, respectively. The flexible linker is highlighted in magenta. The F_1 domain is displayed in gray. Val-334 of subunit α and Asp-315 of subunit β of the F_1 domain form hydrogen bonds with **1a**. (b) Plan for altering the properties of **1a** by attaching one methyl group.

Our continued interest in discovering new natural product analogues with superior functions motivated us to identify potential structural modifications of β-Ala-7–Gly-8 of **1a** to improve its original bioactivity and proteolytic stability (Fig. 2b).[21–25] To minimally perturb the parent structure, we envisioned functionalizing the structure of **1a** with the smallest aliphatic functionality, a methyl group, and designed six methylated analogues **1b–1g**, differing only in the position and configuration of the methyl group. Here we disclose the first solid-phase total synthesis of efrapeptin C (**1a**), the syntheses of **1b–1g**, and a comparison of the physicochemical and biological properties of **1a–1g**. We found that **1f** had a more stabilized 3_{10}-helical conformation, higher hydrophobicity, 4-fold more potent growth inhibition against MCF-7 cells, and higher proteolytic stability than parent **1a**. The present methyl scanning approach led to the discovery of a fully synthetic efrapeptin analogue with superior properties, thereby providing a novel method for changing the intrinsic disadvantages of linear peptidic natural products as pharmaceuticals.[26–31]

domains to contact the target protein. Therefore, structural modifications in β-Ala-7–Gly-8 would potentially alter the entire three-dimensional (3D) structure, the bioactivity, and the proteolytic stability toward the development of new anticancer agents. As the precise functions of the flexible linker are unknown, however, finding analogues with improved properties is neither trivial nor obvious.

The Sewald group reported the total synthesis of **1a** and its analogues by a combination of solution- and solid-phase methods.[18,19] A structure–activity relationship study revealed the significance of β-Ala-7–Gly-8 for the inhibitory activity of **1a** against ATP hydrolysis by the F_1-domain. Attaching a benzyl group to the C3 position of β-Ala-7 led to 10-fold weaker activity and exchanging β-Ala-7 with Aib-7 abolished the activity.[20] Hence, subtle structural changes of the central flexible linker negatively influence the biological properties of **1a**.

Results and discussion

The profound influence of the methyl group on the physico-chemical and biological behaviors has been utilized for developing drug candidates from synthetic small molecules for decades.[32–34] On the other hand, the methyl effect is rarely applied to linear structures in comparison to their cyclic counterparts, presumably due to lower predictability of the appropriate position and orientation of the methyl group for enhancing the original activities. To screen the methyl effect on the conformation, hydrophobicity, bioactivity, and proteolytic stability (Fig. 2b), we aimed to comprehensively install one methyl group to the three methylene sites of β-Ala-7–Gly-8 of **1a** in both (R)- and (S)-configurations, thereby designing six analogues **1b–1g** (Fig. 1). Namely, **1b** (β-Ala-7–L-Ala-8)/**1c** (β-Ala-7–D-Ala-8), **1d** [(R)-β²-hAla-7–Gly-8]/**1e** [(S)-β²-hAla-7–Gly-8], and **1f** [(S)-β³-hAla-7–Gly-8]/**1g** [(R)-β³-hAla-7–Gly-8] are epimeric pairs with one methyl group at the α position of Gly-8, the C2 position of β-Ala-7, and the C3 position of β-Ala-7, respectively.

To investigate the methyl effect on β-Ala-7–Gly-8, we simulated the conformations of **1a–1g** by molecular dynamics (MD). Two thousand structures were randomly generated for each peptide in *n*-octanol using an OPLS3e forcefield, starting from the initial structure that was built based on the protein-bound structure of **1a** (Fig. 2a). To evaluate the impact of the methylated linker, the relative location of the two biologically important helical domains was analyzed (Fig. 3). Specifically, the distance and orientation of residues 1–6 and 9–15 were extracted as the length (r) between the carbonyl carbon atom (B) of L-Leu-6 and the nitrogen atom (C) of Aib-9, and the torsional angle (θ) defined by the α and carbonyl carbon atoms (A–B) of L-Leu-6 and the nitrogen and α carbon atoms (C–D) of Aib-9. The 2000 structures of each peptide were classified by the values of r and θ, plotted as a square dot, and color-coded from blue to red based on the frequency. The r and θ values of the protein-bound conformation of **1a** are 7.7 and 162, respectively (indicated as a pink-colored cross mark. Fig. 3).

According to the area of the colored square dots, the linker conformation of **1a** varied significantly, indicating the unrestricted orientation of the two helical domains. In comparison, the methylated analogues **1b–1g** displayed a narrower conformational distribution than **1a**. The θ values of **1f** with (S)-β³-hAla-7 and its epimer **1g** with (R)-β³-hAla-7 were more localized than those of **1a** or **1b–1e**, indicating that the C3-methyl group of β-Ala-7 had the highest rigidifying effect. The r values of **1b–1f** were mostly smaller than or equivalent to that of the cross mark (7.7 Å), while the r values of **1g** were mostly larger. Thus, the linker of **1b–1f** adopted a more bent conformation than that of

1g. In addition, the color of the square dots revealed that conformations close to the cross mark were frequently found for **1a–1f**, but rarely found for **1g**. It was thus anticipated that **1g** would have weaker bioactivity compared with **1a–1f**, due to a mismatch of its conformation with the protein-bound form. Together, the obtained results clarified that the position and configuration of the methyl group on the linear structure differentially influence the orientation of the two helical domains. Therefore, the linkers of **1b–1g** were expected to effectively modify the original structure and functions of **1a**.

Next, we focused on the syntheses of **1a** and the six methylated analogues **1b–1g** (Fig. 1). To chemically construct **1a–1g** in a unified fashion, we selected a solid-phase strategy over a solution-phase counterpart because of the simplicity of the operations and ease in replacing the monomers for analogue preparations. The solid-phase total synthesis of **1a** had not yet been achieved, and the multiple non-proteinogenic and sterically cumbersome components of **1a** considerably amplify the synthetic challenge. In fact, we faced three major problems during the preliminary study.[35] First, the bulky Aib residues impeded efficient amidation even with the highly reactive reagent combination of *O*-(7-aza-1*H*-benzotriazol-1-yl)-*N,N,N′,N′*-tetramethyluronium hexafluorophosphate (HATU) and 1-hydroxy-7-azabenzotriazole (HOAt).[36] Second, treatment with a strong acid such as trifluoroacetic acid cleaved the peptide sequence at the Pip residues, presumably through oxazolinium ring formation from the carbonyl groups of Pip and the preceding residue in a 1,4-relationship, followed by hydrolysis.[37,38] Third, conjugation of the C-cap was decelerated
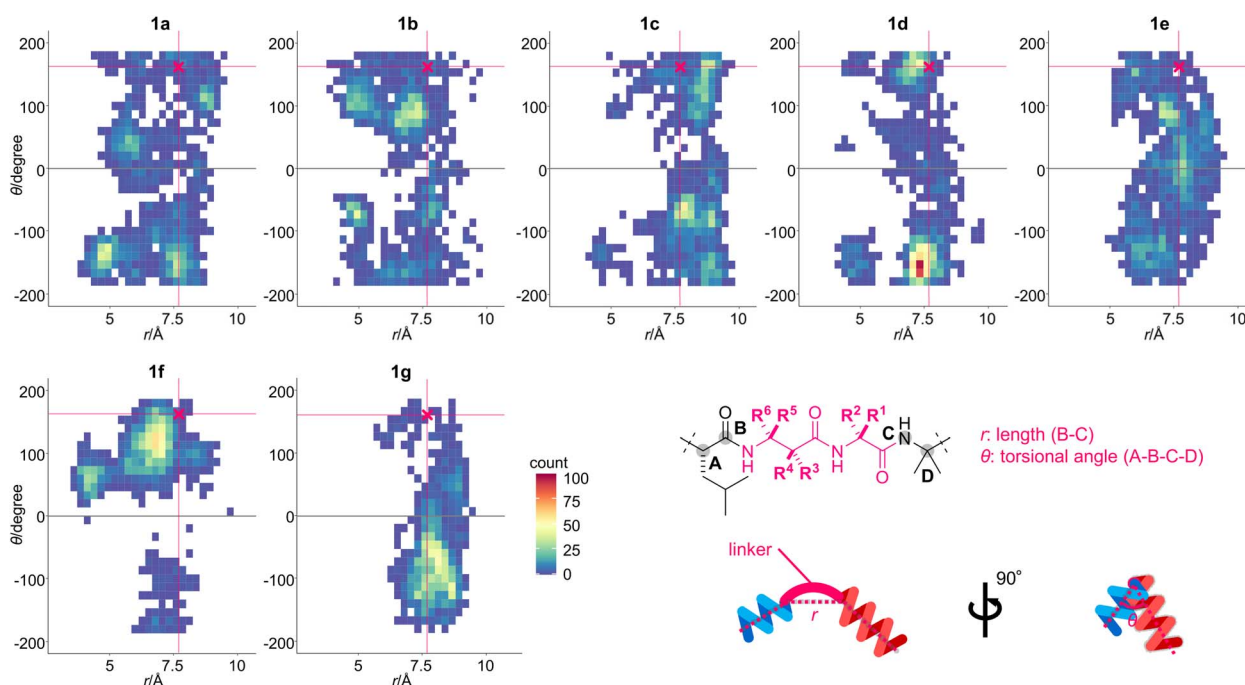

Fig. 3 Two-dimensional histograms of the torsional angle (θ) against the length (r) of **1a–1g**. The 2000 structures for each peptide were generated using a 40 ns trajectory of the replica exchange with solute tempering (REST) simulation in *n*-octanol (OPLS3e forcefield). The initial structure for each peptide was built based on the protein-bound structure of **1a** (PDB ID: 1EFR). The specific conformation of β-Ala-7–Gly-8 was plotted according to r and θ, and the square dots are color-coded according to the obtained frequency. The conformation of **1a** in complex with the F₁-ATP synthase is indicated as a pink-colored cross mark [(r, θ) = (7.7, 162)]. Definitions of r and θ are also shown.

due to the presence of the α,α-dimethyl group of Aib-15 and the sterically encumbered DBN of C-cap.

Retrosynthetically, **1a** and the six methylated analogues **1b–1g** were disassembled into **2–15** (Fig. 4). We planned to start the solid-phase synthesis from resin-linked Fmoc-protected Aib-15 **8**. The acid-labile trityl linker of **8** would allow for peptide release without damaging the acid-sensitive sequence, and the poly(ethylene glycol) (PEG)-based resin (ChemMatrix)[39] of **8** would facilitate coupling of the bulky amino acids due to its high swelling properties in various solvents.[40] Upon elongation, Fmoc-L-Leu-OH (**2**), Fmoc-Gly-OH (**3**), Fmoc-Aib-OH (**4**), Fmoc-L-Pip-OH (**5**), acetic anhydride (**6**), and C-Cap **7** would be utilized as the common structures of all the peptides. Alternatively, Fmoc-β-Ala-OH (**9**) of residue-7 or Fmoc-Gly-OH (**3**) of residue-8 for **1a** was to be replaced with Fmoc-(R)-β^2-hAla-OH (**10**)/Fmoc-(S)-β^2-hAla-OH (**11**) for **1d/1e**, with Fmoc-(S)-β^3-hAla-OH (**12**)/Fmoc-(R)-β^3-hAla-OH (**13**) for **1f/1g**, and with Fmoc-L-Ala-OH (**14**)/Fmoc-D-Ala-OH (**15**) for **1b/1c**. After the release of the sequence, C-cap **7** would be conjugated at the C-terminal Aib-15. To circumvent the unproductive amidation of the bulky Aib residues, the double coupling protocol was applied for attaching Fmoc-Aib-OH (**4**). Moreover, HATU/HOAt was replaced with (1-cyano-2-ethoxy-2-oxoethylidenaminooxy)dimethylaminomorpholinocarbenium hexafluorophosphate (COMU)[41] to form the amide bonds of Aib-2–L-Pip-3, Aib-4–Aib-5, Aib-9–Aib-10, Aib-10–L-Pip-11, and Aib-15–C-cap. The corresponding activated ester of ethyl 2-cyano-2-(hydroxyimino)acetate generated from COMU is less sterically shielded than that of HOAt and thus beneficial for facilitating the coupling of these sterically encumbered components.

The above considerations allowed for the first solid-phase total synthesis of **1a** from Fmoc-protected Aib-15-loaded trityl-ChemMatrix resin **8** (Scheme 1). The first four Fmoc-protected amino acids (**2**, **3**, **4**, and **5**) were condensed by repeating piperidine-mediated Fmoc removal in NMP at 40 °C and HATU/HOAt/i-Pr$_2$NEt-promoted amidation in NMP at 60 °C under microwave irradiation,[42] leading to residues 11–15 **16**. Subsequently, for the stepwise introduction of Fmoc-Aib-OH (**4**) to the secondary amine of Pip-11 and the primary amine of Aib-10, COMU was used as the condensation agent instead of HATU/HOAt. Thus, Fmoc removal and COMU/i-Pr$_2$NEt-promoted elongation of **4** in NMP at 40 °C were performed to attach Aib-10 and Aib-9 to convert **16** to residues 9–15 **18**. Further chain extension from **18** was carried out using **3**, **9**, **2**, and **4** by alternating applications of piperidine and HATU/HOAt/i-Pr$_2$NEt, giving rise to residues 5–15 **19a**. Subsequently, Aib-5 of **19a** was deprotected and reacted with **4** in the presence of COMU to **19a** to provide **20a**. After the Fmoc removal, Aib-4 of **20a** was condensed with **5** using HATU/HOAt to afford **21a**. The ensuing piperidine-treatment and COMU-promoted amidation of **4** converted **21a** to residues 2–15 **22a**. Liberation of the N-terminal amine from **22a** and the HATU/HOAt-mediated amidation with **5** were followed by exchange of the Fmoc group with the acetyl group via sequential treatment with piperidine and Ac$_2$O (**6**), producing acetylated residues 1–15 **23a**. Finally, **23a** was subjected to mildly acidic conditions using (CF$_3$)$_2$CHOH/CH$_2$Cl$_2$ to detach **24a** from the trityl linker without degrading the 15-mer sequence.

The final incorporation of C-cap into the carboxylic acid of **24a** turned out to be a difficult task. Prior to the coupling, amine hydrochloride **7** was neutralized with Et$_3$N to generate the corresponding primary amine, and 10 equivalents of the amine were applied to **24a** in the presence of COMU (10 equiv) and i-Pr$_2$NEt (20 equiv).[35] Whereas the stable azlactone of **25a** was readily formed at the Aib-15 of **24a**, only a minute amount of the desired **1a** was detected after several hours. Hence, we utilized excess amounts of the reagents and extended the reaction time to realize this challenging coupling. Compound **24a** was treated with the free amine of **7** (30 equiv), COMU (20 equiv), and i-Pr$_2$NEt (30 equiv) at 30 °C for 3 d, generating **1a** with the full consumption of azlactone **25a**. Preparative reversed-phase HPLC led to the isolation of pure **1a** in an exceptionally high overall yield (26% over 32 steps from resin **8**). Remarkably, the average yield of each step was approximately 96%, demonstrating the high efficiency of the amidation reactions of the bulky components.

The route from **8** to **1a** was then directly applied to devise the routes to the six methylated analogues **1b–1g** (Scheme 1). Fmoc-(R)-β^2-hAla-OH (**10**), Fmoc-(S)-β^2-hAla-OH (**11**), Fmoc-(S)-β^3-hAla-OH (**12**), and Fmoc-(R)-β^3-hAla-OH (**13**) were employed instead of Fmoc-β-Ala-OH (**9**) of residue-7 of **1a** to prepare **1d**, **1e**, **1f**, and **1g**, respectively. On the other hand, Fmoc-Gly-OH (**3**) of residue-8 of **1a** was replaced with Fmoc-L-Ala-OH (**14**) and Fmoc-D-Ala-OH (**15**) to synthesize **1b** and **1c**, respectively. After HPLC purification, sufficient amounts of **1b–1g** were isolated for further analyses of their physicochemical and biological properties (5.2% for **1b**, 9.4% for **1c**, 4.1% for **1d**, 14% for **1e**, 16% for **1f**, 15% for **1g**), corroborating the robustness of the established synthetic procedure.
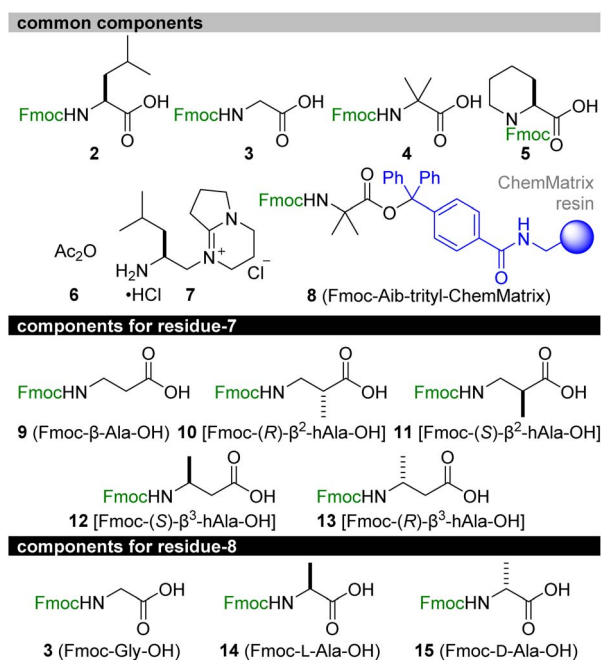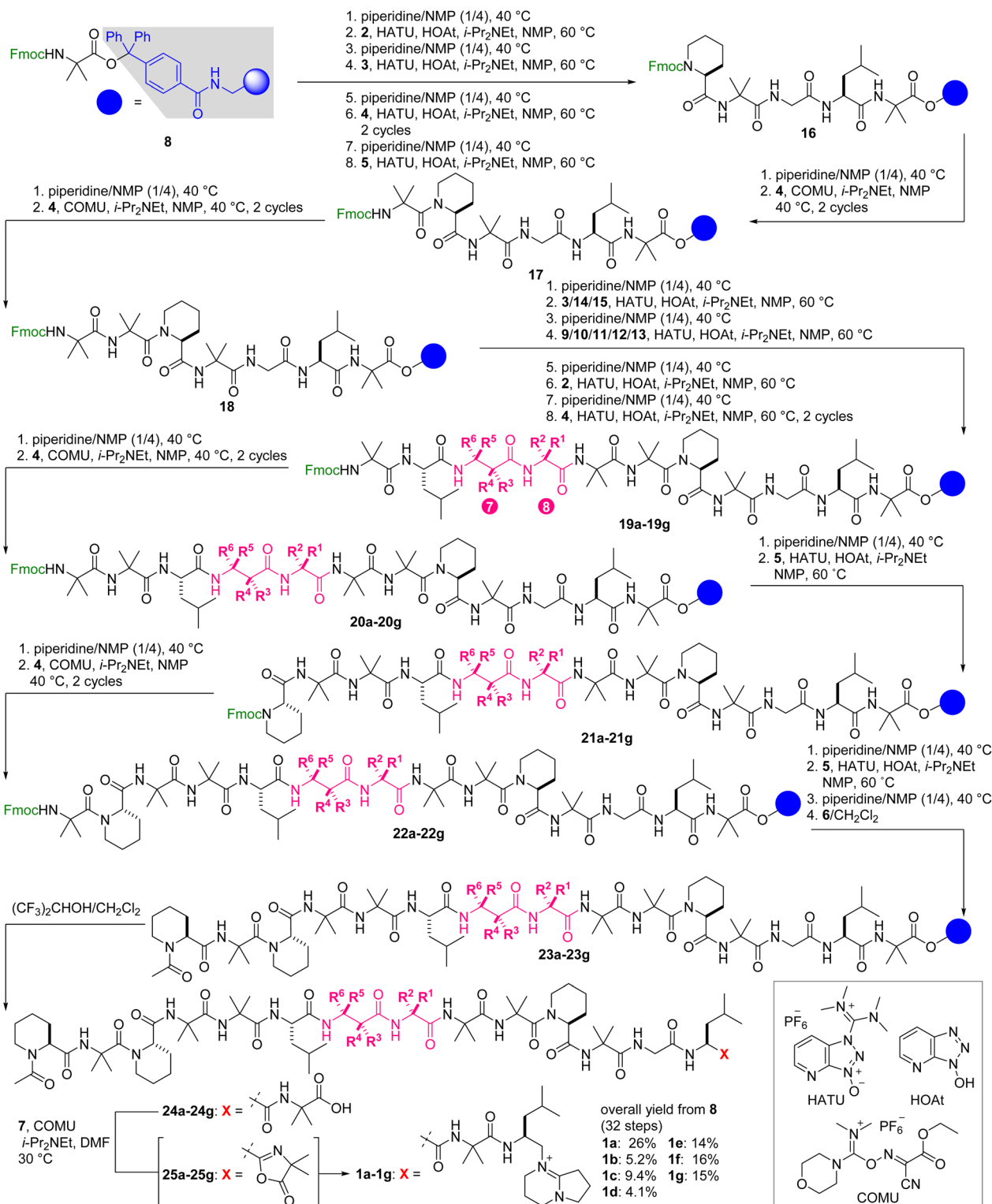

Fig. 4 Synthetic components for total syntheses of **1a–1g**. Fmoc = 9-fluorenylmethoxycarbonyl.

Scheme 1 Solid-phase total syntheses of **1a** and its methylated analogues **1b–1g**. The positions and configurations of methyl groups in compounds **19a–19g**, **20a–20g**, **21a–21g**, **22a–22g**, **23a–23g**, **24a–24g**, and **25a–25g** correspond to those of **1a–1g** displayed in Fig. 1. COMU = (1-cyano-2-ethoxy-2-oxoethylidenaminooxy)dimethylamino-morpholino-carbenium hexafluorophosphate, HATU = O-(7-aza-1H-benzotriazol-1-yl)-N,N,N′,N′-tetramethyluronium hexafluorophosphate, HOAt = 1-hydroxy-7-azabenzotriazole, NMP = N-methyl-2-pyrrolidone.

With the seven fully synthetic peptides in hand, we analyzed the conformation and hydrophobicity of **1a** and six methylated analogues **1b–1g**. To evaluate the folding structures of the seven peptides, electronic circular dichroism (ECD) spectra were measured in CF_3CH_2OH, which is known to mimic a hydrophobic environment of a lipid bilayer (Fig. 5). Natural product
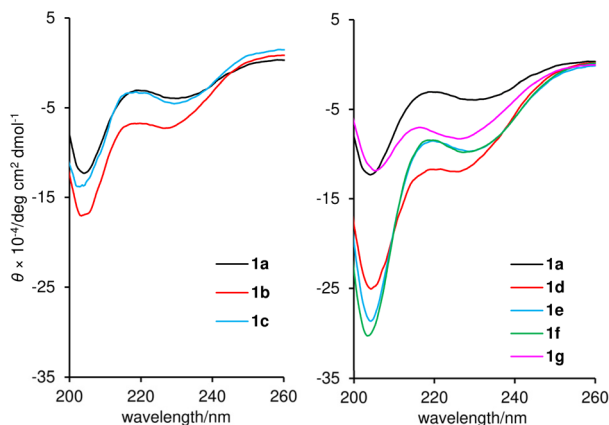
Fig. 5 Electronic circular dichroism (ECD) spectra of **1a–1g**. Data were recorded at a peptide concentration of 61 μM in CF_3CH_2OH.

1a exhibited a large band at 203–206 nm and a small band at 225–235 nm corresponding to the $\pi \rightarrow \pi^*$ and $n \rightarrow \pi^*$ transitions, respectively,[43] thereby confirming the 3_{10}-helical conformations of residues 1–6 and 9–15. Two similar negative bands were observed in the spectra of all the methylated analogues **1b–1g**. Even though the MD simulations indicated the disparate conformational characters of residues 7 and 8 of **1b–1g**, installation of the small methyl group at residue 7 or 8 minimally disturbed the two 3_{10}-helices of **1b–1g**. Interestingly, the intensities of the two bands of **1b**, **1d**, **1e**, and **1f** are higher than those of parent **1a**, and those of **1c** and **1g** are comparable, clarifying the higher helical content of **1b**/**1d**/**1e**/**1f** than **1c**/**1g**. According to the spectra, **1f** and its epimer **1g** have the most and least stabilized 3_{10}-helical structures, respectively. Hence, the configurational switch at the C3-position of β-Ala-7 most significantly influenced the conformational equilibrium of the 3_{10}-helical domains, which should reflect the strongly rigidifying effect of the C3-methyl groups (Fig. 3).

The hydrophobicities of **1a–1g** were estimated by determining the n-octanol/water distribution coefficients (log D). To quantify the log D values, the retention times of the peptides and standard samples with known log D values were compared using ultra high-performance liquid chromatography (UHPLC) equipped with a C18 stationary phase.[44,45] As a result, the log D values were calculated to be 2.03 (**1a**), 2.43 (**1b**), 2.04 (**1c**), 2.11 (**1d**), 2.35 (**1e**), 2.54 (**1f**), and 1.93 (**1g**) (Table 1). Thus, the positions and configurations of the methyl groups modulated the overall hydrophobicity of parent **1a**. The more hydrophobic group, consisting of **1b**, **1d**, **1e**, and **1f**, corresponded to peptides with higher 3_{10}-helical contents. Alternatively, less hydrophobic peptides **1c** and **1g** possessed less stable helical structures. In general, the intramolecular hydrogen bonding associated with helix formation reduces the exposure of the polar amide backbone and increases the hydrophobicity. Thus, we deduced that the diverse hydrophobicity of **1a–1g** originated from the different populations of the 3_{10}-helical conformations indicated by the ECD spectra (Fig. 5).

Next, various biological activities of the six methylated analogues **1b–1g** were assessed and compared with those of **1a**. We first evaluated the ability of **1a–1g** to inhibit ATP synthesis (Table 1). In this assay, intact mitochondria are obtained by permeabilizing the plasma membrane of MCF-7 cells with digitonin and applied to an enzymatic ATP-detection system employing NADP.[46] As the production of NADPH from NADP is coupled with ATP consumption, the amount of ATP synthesized by F_oF_1-ATP synthase can be evaluated from the UV absorbance of NADPH. To standardize the inhibitory activities of **1a–1g**, we calculated the 50% effective concentrations (EC_{50}). Parent **1a** and the five analogues **1b–1f** were similar in their activities, and the EC_{50} values were approximately 1 nM (1.2 nM for **1a**, 1.2 nM for **1b**, 0.86 nM for **1c**, 1.1 nM for **1d**, 0.95 nM for **1e**, and 0.92 nM for **1f**). Thus, the methylation patterns of **1b–1f** had a negligible impact on the inhibition of F_oF_1-ATP synthase because they can adopt the appropriate binding conformation, as predicted by the MD calculations (Fig. 3). In contrast, the

Table 1 Hydrophobicities and biological activities of **1a–1g**

compounds	log D	inhibition of ATP production using cells (EC_{50}, nM)[a,b,c]	growth inhibition[d]		
			JFCR39 (mean GI_{50}, nM)	MCF-7 cells (GI_{50}, nM)[b,c]	MCF-10A cells (GI_{50}, nM)[b,c]
1a	2.03	1.2 ± 0.3	646	37 ± 7	326 ± 125
1b	2.43	1.2 ± 0.4	437	27 ± 8	213 ± 80
1c	2.04	0.86 ± 0.24	1200	104 ± 21**	583 ± 207
1d	2.11	1.1 ± 0.1	933	30 ± 9	323 ± 137
1e	2.35	0.95 ± 0.27	219	14 ± 4	96 ± 50
1f	2.54	0.92 ± 0.17	155	8.8 ± 0.4*	57 ± 31
1g	1.93	2.6 ± 0.1**	2950	173 ± 20**	>1000

log D — hydrophobic / hydrophilic
EC_{50}/GI_{50} — potent / weak

[a] EC_{50} values were determined by evaluating the relative ATP production rate. ATP production rate was calculated from the concentration change within 1 h. [b] Mean values of three independent experiments are displayed with SD. [c] *p < 0.05 and **p < 0.01 determined by Dunnett's test. [d] GI_{50} values were determined by sulforhodamine B assay. The cells were incubated for 48 h.

EC_{50} value of **1g** (2.6 nM) was 2-fold larger than those of **1a–1f**. The lower activity of **1g** would be attributable to the inappropriate 3D orientation of the two helical domains and the lower content of the helical conformations, which were observed in the MD simulation and the ECD spectrum, respectively. Nevertheless, all six methylated analogues **1b–1g** retained the ATP-production inhibitory activities of **1a**.

A JFCR39 cancer panel screening was then conducted to examine the activity profiles of **1a–1g** (Table 1).[47,48] To evaluate the potency of **1a–1g**, mean values of 50% growth inhibition concentrations (GI_{50}) against 39 cancer cell lines were quantified. While the mean GI_{50} value of **1a** was determined to be 646 nM, the strongest **1f** (155 nM) and the weakest **1g** (2950 nM) were 4-fold more and 5-fold less potent than parent **1a**, respectively. Thus, the C3-position of β-Ala-7 was the most effective site for increasing and decreasing the potency of **1a**. Despite the variable potency of **1a–1g**, these seven peptides induced similar response patterns toward the 39 cell lines. For example, HBC-5/MCF-7 (breast), SF-295 (brain), and NCI-H522/DMS114 (lung) cell lines were more susceptible to **1a–1g** than the other tested cell lines. The correlation coefficient values of the response patterns of **1b–1g** turned out to be 0.85–0.90 compared with that of **1a**.[35] Taken together, the panel assays verified that **1b–1g** shared the same mode of action as **1a**.

To more precisely quantify the GI_{50} values, we individually evaluated the growth inhibitory activity of **1b–1g** against **1a**-sensitive MCF-7 cells using a sulforhodamine B assay[49] with 3-fold serial dilutions of peptides (Table 1). The GI_{50} value of parent **1a** was 37 nM in this assay. While all six methylated analogues displayed growth inhibitory activities, **1b–1g** were categorized into the three classes according to their GI_{50} values: **1e** (14 nM) and **1f** (8.8 nM) were stronger analogues, **1b** (27 nM) and **1d** (30 nM) were comparable analogues, and **1c** (104 nM) and **1g** (173 nM) were weaker analogues. Analogue **1f** and its epimer **1g** exhibited 4-fold more and 5-fold less potent activities than **1a**, respectively, and these data were consistent with those of the JFCR39 panel assays. Thus, the configurational switch of the C3-methyl groups of β³-hAla-7 of **1f** and **1g** resulted in a 20-fold difference in the activity. The observed most and least potent activities of **1f** and **1g** are in accordance with their behaviors presumed in Fig. 3, corroborating the predictive power of the MD calculation for the bioactivities. Most importantly, the discovery of the 4-fold more potent analogue **1f** validated the utility of minimum structural modification of the natural product to enhance its bioactivity.

Moreover, we evaluated the cancer cell selectivity of **1a–1g** using the MCF-10A immortalized human breast epithelial cell line as a model of normal cells (Table 1). The GI_{50} values of **1a–1g** against MCF-10A cells were 6 to 11 times greater than those against MCF-7 cells, showing the prominent cancer cell selectivity of **1a–1g**. In particular, the most potent **1f** showed 6-fold more potent growth inhibitory activity against MCF-7 cancer cells (GI_{50} = 8.8 nM) compared with MCF-10A cells (GI_{50} = 57 nM), demonstrating its promising feature as a seed compound of anticancer agents.

While the EC_{50} values of **1a–1g** using mitochondrial F_oF_1-ATP synthase of plasma membrane-permeabilized MCF-7 cells

ranged from 0.86 to 2.6 nM, the GI_{50} values obtained against intact MCF-7 cells ranged from 8.8 to 173 nM. Accordingly, the GI_{50} values not only varied more in terms of the concentration range, but were also at least 10 times higher than the EC_{50} values. We attributed the discrepancy in the two data sets to the distinct hydrophobicities of **1a–1g**. When the log D numbers of **1a–1g** were plotted against $-\log(GI_{50})$ numbers, the points of **1b–1g** displayed a linear relationship ($R^2 = 0.823$) with **1f** and its epimer **1g** being the high and low ends, respectively (Fig. 6). Thus, the more hydrophobic analogues exhibit higher growth inhibition activity. Because increased hydrophobicity generally reduces the barrier to membrane penetration, the analysis suggested the importance of the transportation of **1a–1g** to F_oF_1-ATP synthase. The most potent and hydrophobic **1f** would be most efficiently partitioned into plasma and mitochondrial membranes, and readily transferred to the inner mitochondrial membrane, thereby effectively inhibiting ATP production by F_oF_1-ATP synthase. On the other hand, the least hydrophobic **1g** indeed exhibited the weakest activity, presumably due to the inefficient transportation to the target protein.[50]

Lastly, the methyl effect on proteolytic stability was assessed using parent natural product **1a** and the most potent analogue **1f** to explore their bioavailability. Toward this aim, **1a** and **1f** were subjected to Pronase[51] and papain.[52] Pronase, a mixture of multiple proteases from *Streptomyces griseus*, failed to hydrolyze **1a** or **1f** at 37 °C even after 96 h, uncovering the unusual proteolytic stability of these linear peptides with multiple non-proteinogenic amino acid residues.[35] When papain, a cysteine protease, was utilized, L-BAPA (benzoyl-L-arginine-p-nitro-anilide)[53] was completely degraded at 37 °C within 1 h (Fig. 7). Compounds **1a** and **1f** were significantly more stable than L-BAPA but underwent gradual hydrolysis. After 24 h incubation with papain, 41% of **1a** and 61% of **1f** remained in the reaction solution, which proved the improved protease resistance of **1f**. Inspection of the hydrolyzed peptides of **1a** revealed that hydrolysis occurred at the amide bonds at L-Leu-6–β-Ala-7, Gly-8–Aib-9, and Gly-13–L-Leu-14.[35] Thus, the flexible linker at residues 7–8 was found to be the hot spot of proteolysis of **1a**. Because proteases bind peptides in an extended rather than
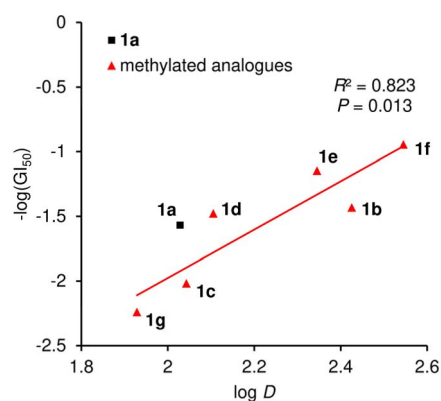

Fig. 6 Plot of $-\log(GI_{50})$ values against log D values of **1a–1g**. The red line represents the linear fit of analogues **1b–1g**. The correlation coefficient (R^2) and P-value are also displayed.
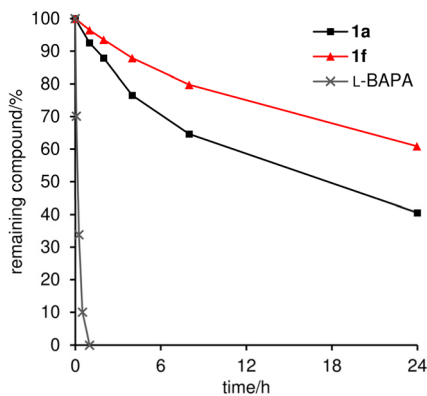
Fig. 7 Proteolytic stability of **1a** and **1f** (71 µM) against papain (0.81 mM). The amount of remaining compound (%) was analyzed during 24 h incubation. L-BAPA = benzoyl-L-arginine-p-nitroanilide.

helical conformation and alkyl groups decelerate the hydrolysis rate, the higher content of the 3_{10}-helical structure and introduction of the C3-methyl group at β-Ala-7 would both contribute to the higher protease stability of **1f**. Consequently, the data demonstrated the superiority of **1f** to parent **1a** as a potential anticancer agent.

Conclusions

In summary, we achieved the first solid-phase total synthesis of efrapeptin C (**1a**), syntheses of the six methylated analogues **1b–1g**, and a detailed evaluation of the physicochemical and biological properties of **1a–1g**. Natural product **1a** possesses seven Aib, three L-Pip residues, and a C-terminal alkylated DBN as the sterically demanding components in its large 15-mer linear sequence. Upon binding to mitochondrial F_oF_1-ATP synthase, Aib-rich residues 1–6 and 9–15 fold into a 3_{10}-helical conformation and β-Ala-7–Gly-8 functions as a flexible linker of the two helical domains. Utilizing the trityl linker for the solid support and COMU as the powerful condensation reagent, we successfully constructed acid-sensitive **1a** with multiple non-proteinogenic monomers in 26% overall yield. Analogues **1b–1g** were then designed to have a single methyl group at β-Ala-7–Gly-8 to modify the original properties of **1a** with minimum structural perturbation. Application of the route to **1a** enabled us to prepare **1b–1g** in a unified fashion, demonstrating the robustness of the devised strategy and tactics. Although **1b–1g** only differ in the position and configuration of one methyl group, the methyl group considerably altered the flexibility of the linker, the stability of the 3_{10}-helix structures, and the hydrophobicities. Compounds **1a–1g** were single-digit nanomolar inhibitors of the ATP production of mitochondrial F_oF_1-ATP synthase, and two- or three-digit nanomolar inhibitors of human breast cancer MCF-7 cell growth, indicating that the original bioactivities of **1a** were maintained in **1b–1g**. The most remarkable analogue was determined to be **1f** with (S)-β³-hAla-7–Gly-8 because it has the most stable 3_{10}-helicity, the highest hydrophobicity, and the most potent activities against cancer cells. Analogue **1f** displayed 4-fold more potent growth

inhibitory activity against MCF-7 cells compared with parent **1a**. The biological analyses suggested that the overall hydrophobicity of **1f** originates from the largest population of the 3_{10}-helical conformation and contributes to the efficient membrane partition before reaching F_oF_1-ATP synthase inside the mitochondria. The cancer cell selectivity of **1f** (MCF-7 vs. MCF-10A) and the superior proteolytic stability of **1f** compared with **1a** further supports the promising role of **1f** as a lead structure for the development of new anticancer agents.

The methyl effect has been used to optimize various properties of numerous drug candidates. It is rarely utilized for conformationally flexible molecules, however, because the effect is not easily predictable. Here we addressed this issue by comprehensively changing the position and configuration of the methyl group of the flexible linker, resulting in the discovery of **1f** with better physicochemical, biological, and proteolytic profiles. The methyl scanning approach demonstrated here will be widely applicable for improving the pharmacologically unfavorable properties of linear peptidic natural products, allowing for the discovery of new drug candidates based on this underappreciated class of compounds.

Data availability

The experimental procedures and additional data can be found in the ESI.†

Author contributions

H. I. and M. I. conceived and designed the study. Y. L. performed the synthesis of compounds and the assays. S. D. performed the cancer panel assay. H. I. and M. I. co-wrote the paper.

Conflicts of interest

There are no conflicts to declare.

Acknowledgements

Notes and references

1 J. Szychowski, J.-F. Truchon and Y. L. Bennani, *J. Med. Chem.*, 2014, **57**, 9292–9308.
2 T. Dang and R. D. Süssmuth, *Acc. Chem. Res.*, 2017, **50**, 1566–1576.

3   D. J. Newman and G. M. Cragg, *J. Nat. Prod.*, 2020, **83**, 770–803.

4   E. Valeur, S. M. Guéret, H. Adihou, R. Gopalakrishnan, M. Lemurell, H. Waldmann, T. N. Grossmann and A. T. Plowright, *Angew. Chem., Int. Ed.*, 2017, **56**, 10294–10323.

5   A. Henninot, J. C. Collins and J. M. Nuss, *J. Med. Chem.*, 2018, **61**, 1382–1414.

6   H. Itoh and M. Inoue, *Chem. Rev.*, 2019, **119**, 10002–10031.

7   A. A. Vinogradov, Y. Yin and H. Suga, *J. Am. Chem. Soc.*, 2019, **141**, 4167–4181.

8   M. Muttenthaler, G. F. King, D. J. Adams and P. F. Alewood, *Nat. Rev. Drug Discovery*, 2021, **20**, 309–325.

9   S. Gupta, S. B. Krasnoff, D. W. Roberts, J. A. A. Renwick, L. S. Brinen and J. Clardy, *J. Am. Chem. Soc.*, 1991, **113**, 707–709.

10 S. Gupta, S. B. Krasnoff, D. W. Roberts, J. A. A. Renwick, L. S. Brinen and J. Clardy, *J. Org. Chem.*, 1992, **57**, 2306–2313.

11 A. R. Bandani, B. P. S. Khambay, J. L. Faull, R. Newton, M. Deadman and T. M. Butt, *Mycol. Res.*, 2000, **104**, 537–544.

12 A. E. Papathanassiu, N. J. MacDonald, D. R. Emlet and H. A. Vu, *Cell Stress Chaperones*, 2011, **16**, 181–193.

13 R. L. Cross and W. E. Kohlbrenner, *J. Biol. Chem.*, 1978, **253**, 4865–4873.

14 For our previous study on yaku'amide B, a new inhibitor of F_oF_1-ATP synthase, see: K. Kitamura, H. Itoh, K. Sakurai, S. Dan and M. Inoue, *J. Am. Chem. Soc.*, 2018, **140**, 12189–12199.

15 For a review of natural product-derived inhibitors of F_oF_1-ATP synthase, see: B. A. Patel, T. L. D'Amico and B. S. J. Blagg, *Eur. J. Med. Chem.*, 2020, **207**, 112779.

16 For the potential utility of OXPHOS inhibitors as anticancer agents, see: Y. Xu, D. Xue, A. Bankhead, III and N. Neamati, *J. Med. Chem.*, 2020, **63**, 14276–14307.

17 J. P. Abrahams, S. K. Buchanan, M. J. Van Raaij, I. M. Fearnley, A. G. Leslie and J. E. Walker, *Proc. Natl. Acad. Sci. U. S. A.*, 1996, **93**, 9420–9424.

18 In the total synthesis of **1a** by the Sewald group, the Aib unit was introduced as 2-azidoacetyl chloride to increase the reactivity for the amidation. In addition, the three synthetic fragments (Ac-L-Pip-1–Gly-8, Aib-9–Gly-13, and L-Leu-14–Aib-15–C-cap) were separately prepared both in solution and on solid phase, and subsequently assembled in solution (8.0% overall yield from the C-cap unit as a starting material). For details, see: M. Jost, J. C. Greie, N. Stemmer, S. D. Wilking, K. Altendorf and N. Sewald, *Angew. Chem., Int. Ed.*, 2002, **41**, 4267–4269.

19 S. Weigelt, T. Huber, F. Hofmann, M. Jost, M. Ritzefeld, B. Luy, C. Freudenberger, Z. Majer, E. Vass, J.-C. Greie, L. Panella, B. Kaptein, Q. B. Broxterman, H. Kessler, K. Altendorf, M. Hollósi and N. Sewald, *Chem.–Eur. J.*, 2012, **18**, 478–487.

20 M. Jost, S. Weigelt, T. Huber, Z. Majer, J. C. Greie, K. Altendorf and N. Sewald, *Chem. Biodiversity*, 2007, **4**, 1170–1182.

21 For our study on enhancing the original bioactivities of peptidic natural products, see ref. 21–23: H. Itoh,

22 K. Tokumoto, T. Kaji, A. Paudel, S. Panthee, H. Hamamoto, K. Sekimizu and M. Inoue, *Nat. Commun.*, 2019, **10**, 2992.

22 Y. Takada, H. Itoh, A. Paudel, S. Panthee, H. Hamamoto, K. Sekimizu and M. Inoue, *Nat. Commun.*, 2020, **11**, 4935.

23 J. Fu, Y. Nakata, H. Itoh, S. Panthee, H. Hamamoto, K. Sekimizu and M. Inoue, *Chem.–Eur. J.*, 2023, **29**, e202301224.

24 For reviews of the structural modification of natural products, see ref. 24 and 25: A. M. Szpilman and E. M. Carreira, *Angew. Chem., Int. Ed.*, 2010, **49**, 9592–9628.

25 Z.-C. Wu and D. L. Boger, *Nat. Prod. Rep.*, 2020, **37**, 1511–1531.

26 Numerous structurally related naturally occurring congeners of **1a** have been reported. The strategy presented here can be directly applied to these compounds. For details, see ref. 26 and 27: T. Degenkolb, J. Kirschbaum and H. Brückner, *Chem. Biodiversity*, 2007, **4**, 1052–1067.

27 A. H. El-Desoky, Y. Hitora, Y. Nishime, Y. Sadahiro, T. Kawahara and S. Tsukamoto, *J. Nat. Med.*, 2024, **78**, 505–513.

28 Since efrapeptins exhibit a wide range of pharmacologically useful functions other than anticancer activity for the development of new pharmaceuticals. For antimalarial activity of efrapeptins, see: G. Nagaraj, M. V. Uma, M. S. Shivayogi and H. Balaram, *Antimicrob. Agents Chemother.*, 2001, **45**, 145–149.

29 For antiviral activity of efrapeptins, see: J. Eichberg, M. Oberpaul, C. Hartwig, A. H. Geißler, C. Culmsee, A. Vilcinskas, E. Böttcher-Friebertshäuser, H. Brückner, T. Degenkolb and K. Hardes, *Arch. Pharm.*, 2024, **357**, e2400384.

30 The β-Ala-Gly linker is not only found in efrapeptins and congeners but also incorporated in PROTAC and radio-labeled molecules. See ref. 30 and 31: S. Wang, Z. Feng, C. Qu, S. Yu, H. Zhang, R. Deng, D. Luo, C. Pu, Y. Zhang and R. Li, *J. Med. Chem.*, 2024, **67**, 9842–9856.

31 A. Ritler, M. S. Shoshan, X. Deupi, P. Wilhelm, R. Schibli, H. Wennemers and M. BéBé, *Bioconjugate Chem.*, 2019, **30**, 657–666.

32 For reviews of the methyl effects in medicinal chemistry, see ref. 26–28: E. J. Barreiro, A. E. Kümmerle and C. A. M. Fraga, *Chem. Rev.*, 2011, **111**, 5215–5246.

33 H. Schönherr and T. Cernak, *Angew. Chem., Int. Ed.*, 2013, **52**, 12256–12267.

34 P. S. M. Pinheiro, L. S. Franco and C. A. M. Fraga, *Pharmaceuticals*, 2013, **16**, 1157.

35 See the ESI† for details.

36 L. A. Carpino, *J. Am. Chem. Soc.*, 1993, **115**, 4397–4398.

37 C. J. Creighton, T. T. Romoff, J. H. Bu and M. Goodman, *J. Am. Chem. Soc.*, 1999, **121**, 6786–6791.

38 C. Rubini, A. Osler, A. Calderan, A. Guiotto and P. Ruzza, *J. Pept. Sci.*, 2008, **14**, 989–997.

39 F. García-Martín, M. Quintanar-Audelo, Y. García-Ramos, L. J. Cruz, C. Gravel, R. Furic, S. Côté, J. Tulla-Puche and F. Albericio, *J. Comb. Chem.*, 2006, **8**, 213–220.

40 S. Lawrenson, M. North, F. Peigneguy and A. Routledge, *Green Chem.*, 2017, **19**, 952–962.

41 A. El-Faham, R. S. Funosas, R. Prohens and F. Albericio, *Chem.–Eur. J.*, 2009, **15**, 9404–9416.

42 S. L. Pedersen, A. P. Tofteng, L. Malik and K. J. Jensen, *Chem. Soc. Rev.*, 2012, **41**, 1826–1844.

43 C. Toniolo, A. Polese, F. Formaggio, M. Crisma and J. Kamphuis, *J. Am. Chem. Soc.*, 1996, **118**, 2744–2745.

44 OECD, *Test No. 117. Partition Coefficient (n-octanol/water), HPLC method, OECD Guidelines for the Testing of Chemicals, Section 1*, OECD Publishing, Paris, 2004.

45 H. Mutoh, Y. Sesoko, T. Kuranaga, H. Itoh and M. Inoue, *Org. Biomol. Chem.*, 2016, **14**, 4199–4204.

46 A. Signorile, L. Micelli, D. De Rasmo, A. Santeramo, F. Papa, R. Ficarella, G. Gattoni, S. Scacco and S. Papa, *Biochim. Biophys. Acta, Mol. Cell Res.*, 2014, **1843**, 675–684.

47 T. Yamori, *Cancer Chemother. Pharmacol.*, 2003, **52**, 74–79.

48 S. Yaguchi, Y. Fukui, I. Koshimizu, H. Yoshimi, T. Matsuno, H. Gouda, S. Hirono, K. Yamazaki and T. Yamori, *J. Natl. Cancer Inst.*, 2006, **98**, 545–556.

49 V. Vichai and K. Kirtikara, *Nat. Protoc.*, 2006, **1**, 1112–1116.

50 The second least potent **1c** exhibited the larger r value than that of the bioactive conformation in the MD simulation, which also supported that the calculation results were consistent with the hydrophobicity.

51 L. L. Cline and M. L. Waters, *Biopolymers*, 2009, **92**, 502–507.

52 Structurally related neoefrapeptin A and N were hydrolyzed by papain. A. Fredenhagen, L.-P. Molleyres, B. Böhlendorf and G. Laue, *J. Antibiot.*, 2006, **59**, 267–280.

53 S. Tokura, N. Nishi and J. Noguchi, *J. Biochem.*, 1971, **69**, 599–600.